JOURNAL OF CHEMICAL INFORMATION AND MODELING

Article

pubs.acs.org/jcim

Differential Binding of Latrunculins to G-Actin: A Molecular Dynamics Study

Mohamed A. Helal,*[,†] Sherief Khalifa,[‡] and Safwat Ahmed[§]

[†]Department of Pharmaceutical Chemistry, Faculty of Pharmacy, Suez Canal University, Ismailia, Egypt

[‡]College of Pharmacy, Qatar University, Doha 02713, Qatar

[§]Department of Pharmacognosy, Faculty of Pharmacy, Suez Canal University, Ismailia, Egypt

Supporting Information

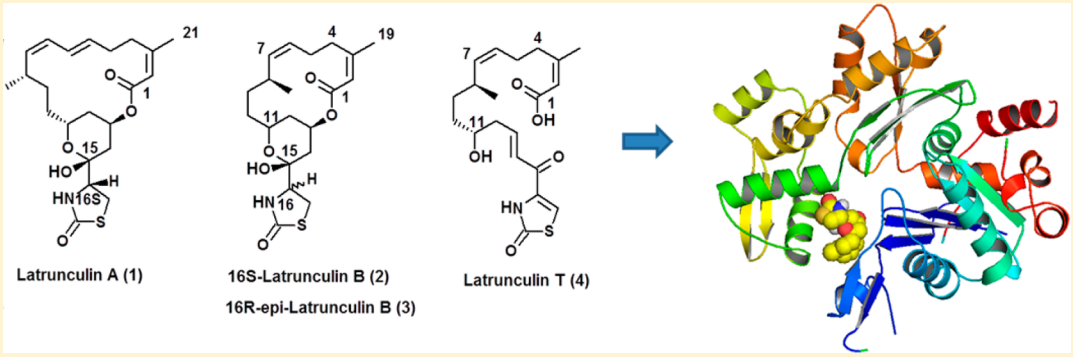

ABSTRACT: Latrunculins are unique macrolides containing a thiazolidinone moiety. Latrunculin A (**1**), latrunculin B (**2**), 16-epi-latrunculin B (**3**), and latrunculin T (**4**) were isolated from the Red Sea sponge *Negombata magnifica*. In the present study, after testing compounds **2**−**4** for cytotoxic activity, they were docked into the crystal structure of G-actin and subjected to binding energy calculation and a 20 ns MD simulation. The modeling study shows that latrunculins binding depends on both hydrophobic interaction of the macrocycle as well as H bonding of the thiazolidinone ring with Asp157 and Thr186. It was noticed that epimerization at C16 of latrunculin B was well tolerated as it could form an alternative H bonding network. However, opening of the macrocyclic ring deteriorates the actin binding due to reduced hydrophobicity. MD simulation showed that latrunculin B (**2**) possesses a more significant stabilizing effect on G-actin than latrunculin T (**4**) and could efficiently hinder the flattening transition of G-actin into F-actin. These findings could explain, at the molecular level, the impact of epimerization and macrolide ring-opening on latrunculins activity, an issue that has not been addressed before. Also, the study gives insights into the mechanism of cytotoxicity of diverse latrunculins and provides direction for future lead optimization studies.

INTRODUCTION

Marine sponges continue to be a rich source of new secondary metabolites with a wide range of biological activities.[1] Over the past years, macrolides of marine origin have continued to be of interest due to their diverse biological properties. One of the macrolide-containing sponges is *Negombata magnifica*. Negombata is represented by four species, two of which are present in the Red Sea, namely, *Negombata magnifica* and *N. corticata*.[2] The Red Sea sponge *Negombata magnifica* (Keller), formerly *Latrunculia magnifica*, family Podospongiidae, was found to emit a reddish fluid which causes fish to retreat. This observation led to the isolation and characterization of two toxin macrolides, latrunculin A (**1**) and B (**2**) (Figure 1).[3,4] Of particular importance, submicromolar quantities of **1** and **2** were found to induce marked reversible changes in cell morphology, disrupt the organization of microfilaments, and suppress microfilament-mediated processes during fertilization and early development.[5−7] At the molecular level, latrunculin A and B were found to bind reversibly to the cytoskeletal protein G-actin and inhibit its polymerization to F-actin.[8−11] Thus, latrunculins are useful probes of actin microfilament structure and function.[11] In addition, latrunculins hold considerable promise as anticancer agents due to their cytotoxicity against various cell lines.[12]

To date, several latrunculins with diverse scaffolds have been isolated, and their biological activities mainly as actin polymerization inhibitors and cytotoxic agents have been proved. In 2008, scientists from the Department of Ocean Sciences, University of California Santa Cruz, classified the reported latrunculins according to the carbon framework into "octaketides" and "heptaketides" represented by latrunculins A (**1**) and latrunculins B (**2**), respectively.[13] These types were further subdivided according to the number of rings due to the presence of some latrunculins with the characteristic macrocyclic loop opened, e.g. latrunculin T (**4**). Another noteworthy

Received: May 28, 2013

   dx.doi.org/10.1021/ci400317j | J. Chem. Inf. Model. XXXX, XXX, XXX−XXX

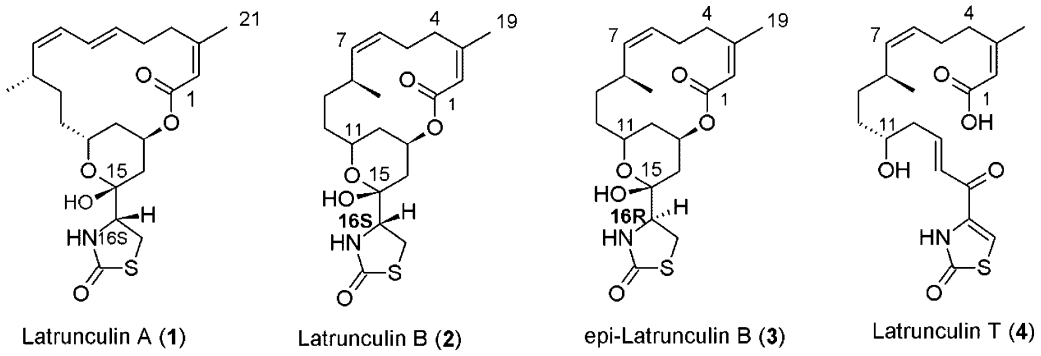

Figure 1. Naturally occurring latrunculins.

chemical feature is the stereochemistry at the point of attachment of the thiazolidinone (TZO) ring (carbon 16 in latrunculins A and B). Examples are latrunculins B (**2**) (16S) and epi-latrunculin B (**3**) (16R). Therefore, we can consider latrunculins A, B, epi-B, and T as representing examples of the diverse latrunculins reported so far. Generally speaking, current literature shows that latrunculin A or its derivatives (octaketides) possess superior actin binding and cytotoxic activities compared to the others. Also, C16 epimerization causes a slight reduction in activity while opening of the macrocycle results in a significant deterioration of the activity.[9,14,15]

Several crystal structures of G-actin complexed with latrunculin A (**1**) and B (**2**) were published as well as docking studies of these compounds and their semisynthetic derivatives.[14,16−18] However, the structure−activity relationship of other latrunculins, especially open-ring latrunculins, and the effect of C16 epimerization and macrocyclic ring-opening on actin binding is still not well understood. In this study, we performed a docking study and binding energy calculation of latrunculin B (**2**), epi-latrunculin B (**3**), and latrunculin T (**4**) in the binding pocket of the G-actin crystal structure in order to study the molecular determinants of their cytotoxic activity. Furthermore, we report for the first time a nanosecond-scale molecular dynamics (MD) simulation study of both latrunculin B and latrunculin T. These computational studies could improve our understanding of the impact of epimerization and ring-opening on latrunculin binding to G-actin and provide valuable insights into the effect of diverse latrunculins on actin dynamics. Surprisingly, few side-by-side biological studies have been conducted on **1**−**4**. Hence, prior to the modeling study, we also reisolated these latrunculins (**1**−**4**) and then evaluated them for their cytoxicity against two types of cell lines.

MATERIALS AND METHODS

i. Bioassay. Two types of cell lines were used throughout this study, human hepatocarcinoma (Hep G2) and human colon cancer cells (HCT-116), obtained from the German Cancer Research Institute. Cells were routinely cultured in Dulbeco's Modified Eagle's Medium (DMEM), except HCT-116 cells, which were grown in McCoy's media. Media were supplemented with 10% fetal bovine serum (FBS), 2 μM L-glutamine, containing 100U/mL penicillin G sodium, 100 U/mL streptomycin sulfate, and 250 ng/mL amphotericin B. Cells were maintained in humidified air containing 5% CO_2 at 37 °C. Monolayer cells were harvested using trypsin/EDTA, except for RAW 264.7 cells, which were collected by scraping. The tested compounds were dissolved in DMSO (99.9%) and diluted 1000-fold in the assays. All experiments were repeated four times, and the data was represented as a Mean (±S.D.). All cell culture material was obtained from Cambrex BioScience (Copenhagen, Denmark). Antitumor activity was estimated by the 3-(4,5-dimethyl-2-thiazolyl)-2,5-diphenyl-2H-tetrazolium bromide (MTT) assay. Cells (5×10^4 cells/well) were incubated overnight in a 96 well plate. Appropriate weights of compounds **2**−**4** were dissolved in DMSO 99.9% to produce 100 μM solution of each compound that was then used for serial dilution. After treatment with various concentrations of the compounds, cells were incubated for 2 h at 37 °C in a serum-free medium, then 40 μL of MTT (5 mg/mL) was added for another 4 h, before addition of 100 μL of acidic isopropyl alcohol (5% HCl). The absorbance was measured at 570 nm using an ELISA reader (BMG Labtechnologies, Durham, NC, USA). The relative cell viability was expressed as the mean percentage of viable cells compared to DMSO-treated cells, and the half maximal growth inhibitory concentration (IC_{50}) was calculated by the trend line equation.

ii. Automated Docking Simulations. Latrunculins **2**−**4** were built and energy-minimized using MMFF charges and the MMFF force field as implemented in Sybyl X.1 with 2000 steps of the conjugate gradient method to a gradient of 0.001 kcal/Å.[19,20] CCDC GOLD 4.12 software was used for docking of the minimized compounds into the putative binding pocket of the G-actin crystal structure PDB: 3SJH.[21] This software uses a genetic algorithm (GA) to explore possible ligand binding modes by changing dihedrals of ligand rotatable bonds, ligand ring geometries, and dihedrals of protein OH and NH_2 groups. The binding site was defined to include all amino acid residues within 10 Å of the side chain oxygen of Glu207 with no distance restraints. Docking was carried out using standard mode settings and GoldScore, a molecular mechanics-like function depending on protein−ligand hydrogen bonding, protein−ligand van der Waals score, ligand intramolecular hydrogen bonding, and ligand intramolecular strain.[22] A total of 10 genetic algorithm runs were performed for each ligand with early termination criteria set to 1.5 Å root-mean-square deviation (RMSD) value.

iii. EMBRACE Calculations. Within the EMBRACE module in Macromodel v9.1 (Schrodinger Inc., Portland, OR, USA), the complexes of **2**−**4** with G-actin were minimized using the OPLS−AA forcefield. A distance-dependent dielectric constant and nonbonded cutoff value of 7.0 Å for vdW and 12.0 Å for electrostatic interactions were used to set up the force field. A conjugate gradient minimization was performed for each complex for 5000 steps until a gradient of 0.001 kJ/ Å. The binding site, including all the residues within 15 Å from

dx.doi.org/10.1021/ci400317j | J. Chem. Inf. Model. XXXX, XXX, XXX−XXX

Arg210, was allowed free movement, while the rest of the protein was kept fixed. EMBRACE calculations were carried out for each complex in both energy difference mode and interaction mode.

iv. Molecular Dynamics Simulation. The Gold generated complexes of latrunculin B and latrunculin T with the G-actin crystal structure (PDB ID: 3SJH) were used for the MD simulation studies. They were individually inserted in a pre-equilibrated TIP3P water orthorhombic box using the system builder tool within the Desmond software as implemented in the Maestro interface (Schrodinger Inc., Portland, OR, USA).[23,24] The size of the box was set to a distance of 15 Å between the boundary and any atom of the protein with a total volume of 828,774 Å^2. To obtain neutral pH conditions, the side chains of lysines and arginines were positively charged, and those of aspartates and glutamates were negatively charged. To attain a net neutral charge, twelve Na^+ ions were added to the system near randomly selected carboxylic groups excluding the binding site (defined as a sphere of 10 Å diameter around the side chain oxygen of Glu207). The water box was composed of 5312 water molecules. MD simulations were carried out using the Desmond application in Maestro, employing the OPLS-AA force field parameters.[25] Prior to the simulation, five steps of minimization were carried out. In the first step, protein and ligand were kept fixed (force constant: 500 kcal/mol/Å^2), and only water and ions were allowed to minimize and relax their positions. During the second step, water, ions, and protein side chains were kept flexible while keeping the protein backbone and ligand restrained with the same force constant. The last three steps involved minimization of the whole system with gradually reducing force constraints of 50, 25, and 10 kcal/mol/Å^2 on the C_α atoms of the backbone. The five minimization steps consisted of 6000 steps each, in which the first 1000 steps were steepest descents, and the last 5000 were Low-memory Broyden-Fletcher-Goldfarb-Shanno (L-BFGS).[26] MD simulations were performed using the minimized structures. The Particle-mesh Ewald (PME) method was used to handle long-range electrostatic interactions.[27] The time step of the simulation was set to 2.0 fs, and a 10 Å cut off was used for nonbonded interactions. The Shake algorithm was employed to keep all bonds involving hydrogen atoms rigid.[28] A constant-volume (NVT) MD simulation was performed for the first 100 ps during which the temperature of the system was raised from 0 → 310 K. The system temperature was maintained at 310 K for the remainder of the simulation using Langevin dynamics. Subsequently, to achieve a smooth relaxation, the system was equilibrated in an NPT ensemble using the same gradually reducing harmonic constraints as in the minimization steps with 200 ps simulation at each step. The production run was then carried out for 20 ns using the NPT ensemble with a target pressure of 1.0132 bar. The evaluation of the trajectory was carried out using Maestro Trajectory Player.

RESULTS AND DISCUSSION

Over the past few years, several latrunculins with diverse chemical structures were isolated, and their biological activities were extensively studied.[12,29,30] A careful literature survey revealed that there are three factors contributing to the diversity of this interesting class of compounds: (i) macrolide ring size, (ii) chirality of the thiazolidine ring or C16 epimerization, and (iii) number of rings or, in other words, macrolide ring-opening.[12−14] We believe that the transition from 16- to 14-membered macrolide ring (macrolide ring size) is now well understood due to the publication of the crystal structures of latrunculins A and B in complex with G-actin.[13,16] However, to our knowledge, no explanation was given for the effect of epimerization or macrolide ring-opening on actin binding. In addition, apart from latrunculin A, there have been no attempts to study the time-dependent behavior of structurally diverse latrunculins in complex with G-actin using molecular dynamic (MD) simulations. To address these issues, we decided to dock **2**−**4** into the binding site of G-actin (10 Å radius from Glu207 side chain oxygen). Then, the complexes obtained were subjected to an EMBRACE energy calculation and MD simulation. These methods could help to delineate the binding modes of diverse latrunculins and understand the effect of epimerization and ring-opening on actin dynamics.

Before proceeding with the modeling study, we reisolated the latrunculins under investigation and performed a quick evaluation of the cytotoxicity of these compounds side-by-side. Flash column chromatography (normal-phase) of the sponge methanol/dichloromethane (1:1) extract provided several fractions. Extensive chromatography afforded **2** as the major metabolite (1.39% of dry weight), while **1**, **3**, and **4** were obtained as minor metabolites. The isolated latrunculins **2**-**4** were evaluated for antitumor activity against two types of tumor cell lines; human colon cancer (HCT-116) and human hepatocarcinoma (Hep G2) using the MTT assay.[31] We noticed that the differences in IC_{50} values seems marginal for colon cancer cells compared to hepatocarcinoma cells. This could be attributed to some differences in cell penetration, metabolism, and/or off-target effects. Cytotoxicity against colon cancer was slightly higher for **2** (IC_{50} 18.62 ± 1.1 μM) and **3** (IC_{50} 19.20 ± 1.8 μM) than for **4** (IC_{50} 20.15 ± 0.6 μM). Also, **2** (IC_{50} 19.27 ± 2.0 μM) was more cytotoxic against hepatocarcinoma than **3** (IC_{50} 25.82 ± 0.9 μM) or **4** (IC_{50} 34.72 ± 2.1 μM) (Figure 1S, Supporting Information). In other words, we noticed that cytotoxic activity follows the order of latrunculin B > epi-latrunculin B > latrunculin T. These results are in line with those reported by El Sayed et al. and Furstner et al. for a series of natural and synthetic latrunculins.[12,14,32] The aforementioned studies showed that 16-epi isomers are slightly less active than the naturally configured analogues, and cleavage of the macrocyclic ring leads to a significant reduction of the activity. It should be noted that the El Sayed study was performed on whole murine brain-metastatic melanoma cells. In vivo and whole-cell assays usually suffer from interference caused by cellular penetration, cell lysis, metabolism, and off-target binding. Also, the actin microfilament disrupting assay reported by Furstner was carried out using only three concentrations of 1, 5, and 10 μM.[12,14] Therefore, there is still a need for a detailed protein assay of the effect of these compounds on the polymerization of G-actin to obtain accurate IC_{50} values. Nevertheless, it is widely accepted that epimerization or macrocyclic ring-opening deteriorates latrunculins activity. We then started our modeling campaign to achieve a better understanding of the SAR of diverse latrunculins, especially, the molecular basis of the effect of macrocyclic ring-opening and C16 epimerization on activity.

i. Binding Modes of Latrunculins. To examine the mode of binding of different latranculins to G-actin and investigate the implications on biological activity, we performed a docking study of **2**−**4** into the binding pocket of this protein. It is worth mentioning that the crystal structure of G-actin complexed with latrunculin B was reported in 2007 (PDB ID: 2Q0U).[17] However, in the present study, we used the highest resolution

dx.doi.org/10.1021/ci400317j | J. Chem. Inf. Model. XXXX, XXX, XXX−XXX

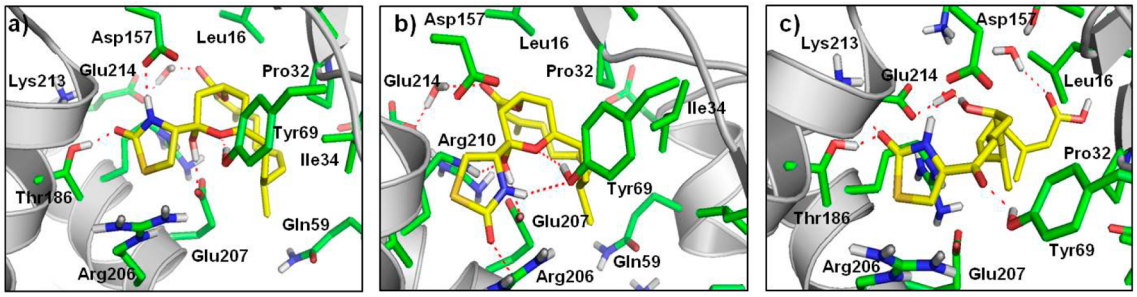

Figure 2. Proposed binding modes of (**a**) latrunculin B (**2**); (**b**) epi-latrunculin B (**3**); and (**c**) latrunculin T (**4**) in G-actin. Backbone is shown as gray helices. Protein side chains are shown as green sticks and bound compound as yellow sticks.

X-ray crystal structure of latrunculin A bound to G-actin (PDB code: 3SJH) for the docking study to avoid bias.[33] All latrunculin derivatives studied were docked into the same binding site of latrunculin A in the aforementioned crystal structure using CCDC Gold software. Previously reported crystal structures of latrunculins A and B in G-actin show that latrunculins bind in a hydrophobic binding cleft between subdomains 2 and 4 with the polar 5-membered ring directed toward a polar pocket close to the nucleotide binding site.[10,33,34] This orientation allows latrunculins to inhibit the conformational changes necessary for actin filament polymerization. As expected, in our docking study, **2** showed more favorable interactions than **3** or **4**, with GOLD docking scores of 85.97, 64.17, and 53.52, respectively (detailed scores are given in Table S1, Supporting Information).

The docked conformation of **2** shared a very similar binding mode to the reported crystal structure (PDB ID: 2Q0U) with an RMSD of only 0.203. The polar part of the molecule forms an extensive network of H bonds (Figure 2a). The carbonyl group of the TZO ring shows an H bond with Thr186, while the NH forms a shorter H bond with Asp157. The hydroxy group has 2 H bonds with Glu207 and Arg210 in similarity to the crystal structure. Also, the oxygen of the tetrahydropyran ring is involved in a strong H bond with Tyr69. Finally, the hydrophobic macrocycle was found to adopt a conformation complementary to the hydrophobic surface created by residues Leu16, Pro32, and Ile34.

The naturally occurring isomer, 16-epi-latrunculin B (**3**), shared a comparable binding pattern with latrunculin B (**2**), particularly in its macrocyclic hydrophobic loop. However, the polar TZO ring was flipped bringing its NH and carbonyl oxygen away from Asp157 and Thr186, the amino acids involved in H bonding in case of latrunculin B. Instead, this ring NH and carbonyl group form two weaker H bonds with Tyr69 and Arg206, respectively (Figure 2b). In addition, the obvious internal strain in the docked conformation of 16-epi-latrunculin B was found to deteriorate its docking score. These factors provide a partial explanation for the weaker actin binding of 16-epilatrunculin B (**3**), compared to latrunculin B (**2**).

Finally, latrunculin T (**4**) was docked into the same binding site without any constraints. Interestingly, the polar head of latrunculin T showed the same H bonding network as latrunculin B (**2**) (Figure 2c). In addition, the lactone carbonyl group next to the polar head forms a weak H bond with Tyr69. However, despite an extensive H bonding network, **4** shows a reduced docking score compared to **2** which is likely due to the reduced hydrophobicity of the opened lactone ring and hence a lower contribution to its steric component (44.70 for **4**; 53.62 for **2**, Table S1, Supporting Information). Also, the higher internal strain in **4** has a negative contribution to the overall score (−14.33 for **4**, −4.55 for **2**). Furthermore, we assume that the less flexible and more hydrophobic **2** loses less entropy upon binding than **4**.

ii. EMBRACE Calculations. The GOLD-derived complexes of **2**, **3**, and **4** with G-actin were subjected to the automated mechanism of multiligand bimolecular association with energetics (EMBRACE) minimization within Macromodel v9.1. Calculations were performed for each complex in both "energy difference mode" and "interaction energy mode". The first mode calculates the minimized energy of both the separate ligand and protein subtracted from the minimized energy of the whole complex to estimate energy changes upon association. The energy difference is then calculated using the following equation:

$$\Delta E = E_{complex} - E_{ligand} - E_{protein}$$

The "interaction energy mode" separates the atoms in the ligand and the receptor into two sets and then calculates the interaction energy between them providing the EMBRACE scores given in Table 1. As expected, in both types of calculations, the latrunculin B complex gave better scores than the epi-latrunculin B complex followed by the latrunculin T complex. This was found to be mainly due to the van der Waals component of the score as all ligands show similar electrostatic contacts with the receptor. The scores of the EMBRACE calculations comply with the outcomes of the modeling study and give more emphasis to the molecular basis of the activity of these compounds.

Table 1. EMBRACE Scores for Latrunculin B and T Complexes with G-Actin

	energy difference	interaction energy
latrunculin B complex	−212.73	−426.83
epi-latrunculin B	−177.63	−405.45
latrunculin T complex	−117.09	−290.72

iii. Molecular Dynamics Simulation. In addition to the docking studies and binding energy calculations, we decided to perform an MD simulation of the crystal structure of G-actin (PDB: 3SJH) in complex with different latrunculins. Notably, the MD simulation of latrunculin A was recently reported using the crystal structure of inhibitor-bound actin (PDB: 1ESV).[10,35] In the present study, we investigated the binding modes and the time-dependent behavior of other biologically important latrunculins (B and T) using a higher resolution crystal structure of G-actin (PDB: 3SJH). This approach should allow for a better understanding of the structure−activity relation-

dx.doi.org/10.1021/ci400317j | J. Chem. Inf. Model. XXXX, XXX, XXX−XXX

ships of this class of compounds and reveal new insights into the effect of epimerization and macrolide ring-opening on actin dynamics and function.

The GOLD-derived complexes of latrunculins B and T were embedded in a rectangular box of pre-equilibrated water molecules. These systems were then equilibrated and simulated for 20 ns each in an NPT ensemble using the Desmond software. A side view of the G-actin-latrunculin B complex after the 20 ns MD simulation is shown in Figure 3. Several

Figure 3. G-actin-latrunculin B complex. The protein helices are shown as colored cartoons, while (**2**) is shown as spheres with yellow carbons.

parameters could be monitored during the simulation to confirm the physical stability of the system, such as backbone root-mean-square deviation (RMSD) and potential energy. It was noticed that the potential energy of both systems decreased initially during the first 5−7 ns and then stabilized over the rest of simulation (data not shown). Also, the C_α RMSD from the initial G-actin structure showed adequate stability over the course of the MD simulation (discussed later). The low RMSD fluctuation of the simulated systems indicates the suitability of the equilibration and simulation protocols applied. For both systems, the final complex was minimized and visually inspected to ensure the presence of key interactions between the ligands and binding site residues.

Binding Mode Stability of Different Latrunculins. The binding modes of **2** and **4** were monitored during the whole MD simulation using the Maestro Trajectory Player and by calculating the exact intermolecular distances. This helped to examine the stability of the proposed H bonds as well as the distances to the binding site residues. As mentioned above, **2** showed an extensive H bonding network that was stable during the entire MD simulation. The H bond between the TZO NH and Asp157 remained stable around 1.5 Å as well as the H-bond between the hydroxy group and Glu207 which showed a slightly longer distance with an average of 1.6 Å (Figure 4). Although the interaction between the latrunculin B carbonyl and Thr186 suffered from significant fluctuation, it remained within the H bonding range. It was also noticed that appropriate shape complementarity was maintained during the simulation between the macrocyclic ring of latrunculins B and the hydrophobic pocket residues with an average distance of 4.2 Å from Leu16 (data not shown). Interestingly,

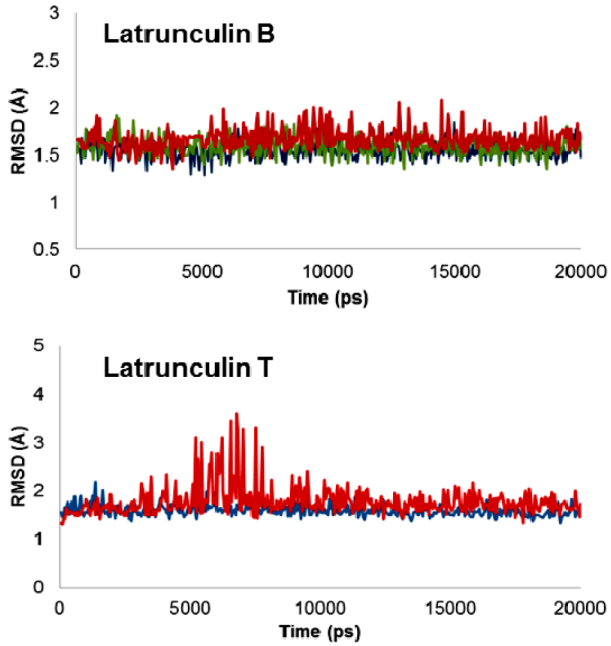

Figure 4. H bond distances between latrunculins B and T and important binding site polar residues. Red: TZO C═O−Thr186, Blue: TZO NH−Asp157, Green: latrunculin B OH—Glu207.

latrunculin T showed very similar H bond stability with a stronger NH-Asp157 interaction (∼1.5 Å). On the other hand, the H bond between the TZO carbonyl and Thr186 showed higher fluctuations and was broken between 5 and 8 ns. The smaller hydrophobic tail of latrunculin T undergoes significant fluctuation and was not able to occupy the hydrophobic pocket formed by Leu16, Val30, Pro32, and Ile34 throughout the entire MD simulation.

Stabilizing Effect on G-Actin Interdomain Motion. We investigated the effect of binding of **2**−**4** on the dynamic behavior of G-actin. The RMSD of both studied systems with respect to the initial conformation of the G-actin complex was monitored during the simulation. For the latrunculin B complex, the C_α RMSD increases steadily during the first 5 ns and then stabilizes at less than 1 Å. This indicates that latrunculin B binding allows minor fluctuations of the actin backbone (on the ns time scale). On the other hand, the G-actin−latrunculin T complex shows a more pronounced movement with a C_α RMSD average of 1.75 Å during the last 10 ns of the simulation that was comparable to the movement of the free G-actin (Figure 5a).

Finally, we studied the dynamic properties of the backbone of the "hinge region". The part of the G-actin structure as described by Oda et al. involved in the flattening of the protein during its transition to F-actin.[36] The bending residues forming the hinge region were determined by DynDom software (Steven Hayward, University of East Anglia, UK) for protein motion analysis using the crystal structures of G and F actin (PDB: 1J6Z and 2ZWH, respectively).[37] The RMSD of the backbone atoms of the bending residues (141, 142, and 337−341) was monitored for free G-actin and for the protein in complex with latrunculin B and T. As expected, the hinge region residues of the latrunculin T complex showed higher RMSD values and fluctuations compared to the latrunculin B complex with an average difference of 0.5 Å (Figure 5b). In this case, the RMSD of the latrunculin T hinge region was slightly

dx.doi.org/10.1021/ci400317j | J. Chem. Inf. Model. XXXX, XXX, XXX−XXX

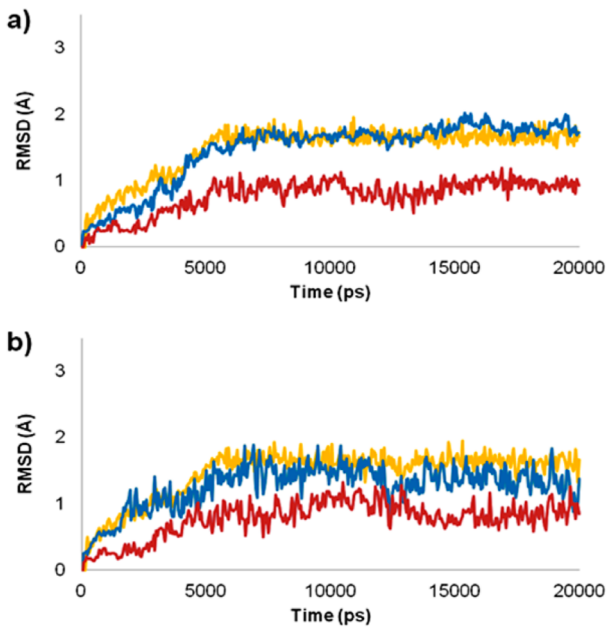

Figure 5. Monitored RMSD during the 20 ns MD simulation. **a)** C_α RMSD of the free G-actin (yellow) and G-actin in complex with latrunculin B (red) and latrunculin T (blue). **b)** Backbone RMSD of bending residues of the free G-actin (yellow) and G-actin in complex with latrunculin B (red) and latrunculin T (blue).

lower than that of the free G-actin, but the difference is insignificant. Together, these results indicate that latrunculin B possesses a more significant stabilizing effect on the G-actin movement and could efficiently hinder the flattening transition of G-actin into F-actin. As evident from the docking and MD simulation studies, both latrunculin B and T show an extensive H bonding network with Asp157, Thr186, Glu207, and/or Tyr69. Therefore, we assume that the difference of their effects on actin dynamics is mainly attributed to steric factors. The relatively rigid lactone ring of latrunculin B adopts a complementary conformation to the hydrophobic pocket of G-actin. Therefore, it could act as a wedge between the G-actin subdomains hindering the interdomain rotation.

CONCLUSIONS

The aim of this study was to understand the effect of epimerization and macrolide ring-opening on several latrunculins binding to G-actin. Latrunculin B (**2**), epi-latrunculin B (**3**), and latrunculin T (**4**) were isolated and evaluated for cytotoxic activity against two different human cancer cell lines. Latrunculins (**2**-**4**) were docked into the crystal structure of G-actin and subjected to EMBRACE calculation and, for the first time, to a 20 ns MD simulation allowing for a comprehensive understanding of their structure−activity relationships. Our results indicate that binding of these compounds to actin depends mainly on two types of interactions, hydrogen bonding with the polar TZO ring and hydrophobic interactions with the macrocycle. When the macrolide ring is opened, the cytotoxic activity is compromised. Also, we showed in a previous study that any substitution on the polar H bonding groups of latrunculins would significantly deteriorate actin binding.[38] On the other hand, we illustrated that inversion of C16 is well tolerated as the polar head is able to form alternative H bonds with Tyr69 and Arg206. Nevertheless, a comprehensive 3D-QSAR study for the isolated latrunculins has yet to be reported. Insights gained from this study could aid in the design of synthetic latrunculins for anticancer chemotherapy.

ASSOCIATED CONTENT

Supporting Information

Procedures for latrunculin isolation, activity graphs, and detailed docking score. This material is available free of charge via the Internet at http://pubs.acs.org.

AUTHOR INFORMATION

Corresponding Author

*Phone: +2-0120-1122213. Fax: +2-064-3230741. E-mail: mohamedahelal@gmail.com, mohamed_hilal@pharm.suez.edu.eg.

Notes

The authors declare no competing financial interest.

ACKNOWLEDGMENTS

The authors wish to acknowledge the Egyptian Environmental Affairs Agency (EEAA) for facilitating sample collection along the coasts of the Red Sea. The authors are grateful to Professor Robert W. M. Van Soest, the Faculty of Science of The Zoological Museum of Amsterdam for taxonomic identification of the sponge. Human hepatocarcinoma (Hep-G2) and human colon cancer cells (HCT-116) were a generous gift from the German Cancer Research Institute, Heidelberg, Germany.

REFERENCES

(1) Blunt, J. W.; Copp, B. R.; Munro, M. H.; Northcote, P. T.; Prinsep, M. R. Marine natural products. *Nat. Prod. Rep.* **2003**, *20*, 1−48.

(2) Vilozny, B.; Amagata, T.; Mooberry, S. L.; Crews, P. A new dimension to the biosynthetic products isolated from the sponge Negombata magnifica. *J. Nat. Prod.* **2004**, *67*, 1055−7.

(3) Kashman, Y. G., A.; Shmueli, U. Latrunculin, a new 2-thiazolidinone macrolide from the marine sponge Latrunculia magnifica. *Tetrahedron Lett.* **1980**, *21*, 3629−3632.

(4) Groweiss, A. S. U.; Kashman, Y. Marine toxins of Latrunculia magnifica. *J. Org. Chem.* **1983**, *48*, 3512−3516.

(5) Foissner, I.; Wasteneys, G. O. Wide-ranging effects of eight cytochalasins and latrunculin A and B on intracellular motility and actin filament reorganization in characean internodal cells. *Plant Cell Physiol.* **2007**, *48*, 585−597.

(6) Ayscough, K. R.; Stryker, J.; Pokala, N.; Sanders, M.; Crews, P.; Drubin, D. G. High rates of actin filament turnover in budding yeast and roles for actin in establishment and maintenance of cell polarity revealed using the actin inhibitor latrunculin-A. *J. Cell Biol.* **1997**, *137*, 399−416.

(7) Spector, I.; Shochet, N. R.; Kashman, Y.; Groweiss, A. Latrunculins: novel marine toxins that disrupt microfilament organization in cultured cells. *Science* **1983**, *219*, 493−495.

(8) Terashita, Y.; Wakayama, S.; Yamagata, K.; Li, C.; Sato, E.; Wakayama, T. Latrunculin A can improve the birth rate of cloned mice and simplify the nuclear transfer protocol by gently inhibiting actin polymerization. *Biol. Reprod.* **2012**, *86*, 180.

(9) Khanfar, M. A.; Youssef, D. T.; El Sayed, K. A. 3D-QSAR studies of latrunculin-based actin polymerization inhibitors using CoMFA and CoMSIA approaches. *Eur. J. Med. Chem.* **2010**, *45*, 3662−3668.

(10) Morton, W. M.; Ayscough, K. R.; McLaughlin, P. J. Latrunculin alters the actin-monomer subunit interface to prevent polymerization. *Nat. Cell Biol.* **2000**, *2*, 376−378.

(11) Coue, M.; Brenner, S. L.; Spector, I.; Korn, E. D. Inhibition of actin polymerization by latrunculin A. *FEBS Lett.* **1987**, *213*, 316−318.

(12) El Sayed, K. A.; Youssef, D. T.; Marchetti, D. Bioactive natural and semisynthetic latrunculins. *J. Nat. Prod.* **2006**, *69*, 219−223.

(13) Amagata, T.; Johnson, T. A.; Cichewicz, R. H.; Tenney, K.; Mooberry, S. L.; Media, J.; Edelstein, M.; Valeriote, F. A.; Crews, P. Interrogating the bioactive pharmacophore of the latrunculin chemotype by investigating the metabolites of two taxonomically unrelated sponges. *J. Med. Chem.* **2008**, *51*, 7234−7242.
(14) Furstner, A.; Kirk, D.; Fenster, M. D.; Aissa, C.; De Souza, D.; Nevado, C.; Tuttle, T.; Thiel, W.; Muller, O. Latrunculin analogues with improved biological profiles by "diverted total synthesis": preparation, evaluation, and computational analysis. *Chemistry* **2007**, *13*, 135−149.
(15) Sayed, K. A.; Khanfar, M. A.; Shallal, H. M.; Muralidharan, A.; Awate, B.; Youssef, D. T.; Liu, Y.; Zhou, Y. D.; Nagle, D. G.; Shah, G. Latrunculin A and its C-17-O-carbamates inhibit prostate tumor cell invasion and HIF-1 activation in breast tumor cells. *J. Nat. Prod.* **2008**, *71*, 396−402.
(16) Didry, D.; Cantrelle, F. X.; Husson, C.; Roblin, P.; Moorthy, A. M.; Perez, J.; Le Clainche, C.; Hertzog, M.; Guittet, E.; Carlier, M. F.; van Heijenoort, C.; Renault, L. How a single residue in individual beta-thymosin/WH2 domains controls their functions in actin assembly. *EMBO J.* **2012**, *31*, 1000−1013.
(17) Allingham, J. S.; Miles, C. O.; Rayment, I. A structural basis for regulation of actin polymerization by pectenotoxins. *J. Mol. Biol.* **2007**, *371*, 959−970.
(18) Khanfar, M. A.; Youssef, D. T.; El Sayed, K. A. Semisynthetic latrunculin derivatives as inhibitors of metastatic breast cancer: biological evaluations, preliminary structure-activity relationship and molecular modeling studies. *ChemMedChem* **2010**, *5*, 274−285.
(19) Clark, M.; Cramer, R. D., III; Van Opdenbosch, N. Validation of the general purpose tripos 5.2 force field. *J. Comput. Chem.* **1989**, *10*, 982−991.
(20) Halgren, T. A. Merck molecular force field. I. Basis, form, scope, parametization, and performance of MMFF94. *J. Comput. Chem.* **1996**, *17*, 490−519.
(21) Jones, G.; Willett, P.; Glen, R. C.; Leach, A. R.; Taylor, R. Development and validation of a genetic algorithm for flexible docking. *J. Mol. Biol.* **1997**, *267*, 727−748.
(22) Annamala, M. K.; Inampudi, K. K.; Guruprasad, L. Docking of phosphonate and trehalose analog inhibitors into M. tuberculosis mycolyltransferase Ag85C: Comparison of the two scoring fitness functions GoldScore and ChemScore, in the GOLD software. *Bioinformation* **2007**, *1*, 339−350.
(23) Huggins, D. J. Correlations in liquid water for the TIP3P-Ewald, TIP4P-2005, TIP5P-Ewald, and SWM4-NDP models. *J. Chem. Phys.* **2012**, *136*, 064518.
(24) Bowers, K. J.; Chow, E.; Xu, H.; Dror, R. O.; Eastwood, M. P.; Gregersen, B. A.; Klepeis, J. L.; Kolossvary, I.; Moraes, M. A.; Sacerdoti, F. D.; Salmon, J. K.; Shan, Y.; Shaw, D. E. Scalable algorithms for molecular dynamics simulations on commodity clusters. Proceedings of the 2006 ACM/IEEE Conference on Supercomputing (SC06), Tampa, FL, 11 to 17 November 2006, ACM Press, New York, 2006.
(25) Jorgensen, W. L.; Tirado-Rives, J. The OPLS [optimized potentials for liquid simulations] potential functions for proteins, energy minimizations for crystals of cyclic peptides and crambin. *J. Am. Chem. Soc.* **1988**, *110*, 1657−1666.
(26) Stewart, J. J. Application of the PM6 method to modeling proteins. *J. Mol. Model.* **2009**, *15*, 765−805.
(27) Isele-Holder, R. E.; Mitchell, W.; Ismail, A. E. Development and application of a particle-particle particle-mesh Ewald method for dispersion interactions. *J. Chem. Phys.* **2012**, *137*, 174107.
(28) Hauptman, H. A. Shake-and-bake: an algorithm for automatic solution ab initio of crystal structures. *Methods Enzymol.* **1997**, *277*, 3−13.
(29) Gronewold, T. M.; Sasse, F.; Lunsdorf, H.; Reichenbach, H. Effects of rhizopodin and latrunculin B on the morphology and on the actin cytoskeleton of mammalian cells. *Cell Tissue Res.* **1999**, *295*, 121−129.
(30) Houssen, W. E.; Jaspars, M.; Wease, K. N.; Scott, R. H. Acute actions of marine toxin latrunculin A on the electrophysiological properties of cultured dorsal root ganglion neurones. *Comp. Biochem. Physiol., Part C: Toxicol. Pharmacol.* **2006**, *142*, 19−29.
(31) Hansen, M. B.; Nielsen, S. E.; Berg, K. Re-examination and further development of a precise and rapid dye method for measuring cell growth/cell kill. *J. Immunol. Methods* **1989**, *119*, 203−210.
(32) Furstner, A.; Kirk, D.; Fenster, M. D.; Aissa, C.; De Souza, D.; Muller, O. Diverted total synthesis: preparation of a focused library of latrunculin analogues and evaluation of their actin-binding properties. *Proc. Natl. Acad. Sci. U. S. A.* **2005**, *102*, 8103−8108.
(33) Gaucher, J. F.; Mauge, C.; Didry, D.; Guichard, B.; Renault, L.; Carlier, M. F. Interactions of isolated C-terminal fragments of neural Wiskott-Aldrich syndrome protein (N-WASP) with actin and Arp2/3 complex. *J. Biol. Chem.* **2012**, *287*, 34646−34659.
(34) Tsurumura, T.; Tsumori, Y.; Qiu, H.; Oda, M.; Sakurai, J.; Nagahama, M.; Tsuge, H. Arginine ADP-ribosylation mechanism based on structural snapshots of iota-toxin and actin complex. *Proc. Natl. Acad. Sci. U. S. A.* **2013**, *110*, 4267−4272.
(35) Rennebaum, S.; Caflisch, A. Inhibition of interdomain motion in G-actin by the natural product latrunculin: a molecular dynamics study. *Proteins* **2012**, *80*, 1998−2008.
(36) Oda, T.; Maeda, Y. Multiple conformations of F-actin. *Structure* **2010**, *18*, 761−767.
(37) Hayward, S.; Berendsen, H. J. Systematic analysis of domain motions in proteins from conformational change: new results on citrate synthase and T4 lysozyme. *Proteins* **1998**, *30*, 144−154.
(38) Kudrimoti, S.; Ahmed, S. A.; Daga, P. R.; Wahba, A. E.; Khalifa, S. I.; Doerksen, R. J.; Hamann, M. T. Semisynthetic latrunculin B analogs: studies of actin docking support a proposed mechanism for latrunculin bioactivity. *Bioorg. Med. Chem.* **2009**, *17*, 7517−7522.